J Neuropathol Exp Neurol

Vol. 68, No. 11
November 2009
pp. 1207–1218

ORIGINAL ARTICLE

A Novel *Caspr* Mutation Causes the Shambling Mouse Phenotype by Disrupting Axoglial Interactions of Myelinated Nerves

Xiao-yang Sun, PhD, Yoshiko Takagishi, PhD, Erina Okabe, MSc, Yûko Chishima, BSc, Yasuhiko Kanou, PhD, Shiori Murase, DVM, Kazue Mizumura, MD, PhD, Mie Inaba, MD, Yukio Komatsu, MD, PhD, Yoshitaka Hayashi, MD, PhD, Elior Peles, PhD, Sen-ichi Oda, PhD, and Yoshiharu Murata, MD, PhD

Abstract

The neurological mouse mutation shambling (*shm*) exhibits ataxia and hindlimb paresis. Positional cloning of *shm* showed that it encodes contactin-associated protein (Caspr), which is required for formation of the paranodal junction in myelinated nerves. The *shm* mutation is a TT insertion in the *Caspr* gene that results in a frame shift and a premature stop codon at the COOH-terminus. The truncated Caspr protein that is generated lacks the transmembrane and cytoplasmic domains. Here, we found that the nodal/paranodal axoplasm of *shm* mice lack paranodal junctions and contain large mitochondria and abnormal accumulations of cytoplasmic organelles that indicate altered axonal transport. Immunohistochemical analysis of mutant mice showed reduced expression of Caspr, contactin, and neurofascin 155, which are thought to form a protein complex in the paranodal region; protein 4.1B, however, was normally distributed. The mutant mice had aberrant localization of voltage-gated ion channels on the axolemma of nodal/paranodal regions. Electrophysiological analysis demonstrated that the velocity of saltatory conduction was reduced in sciatic nerves and that the visual response was attenuated in the primary visual cortex. These abnormalities likely contribute to the neurological phenotype of the mutant mice.

Key Words: Contactin-associated protein, Myelin, Optic nerves, Paranodes, Sciatic nerves.

INTRODUCTION

Saltatory conduction of nerve impulses in myelinated nerves depends on highly specialized axonal domains termed the *node of Ranvier*, the *paranode*, the *juxtaparanode*, and the *internode*. The paranodes flanking the node of Ranvier are one of the major attachment sites between the axon and myelinating glial cells, that is, oligodendrocytes in the central nervous system (CNS) and Schwann cells in the peripheral nervous system (PNS) (1–5). A septate-like adhesive junction is formed at the paranode between the axolemma and myelin loops. The paranode acts as an electrical and a biochemical barrier between nodal and internodal membrane compartments. In addition, the paranodal junction is thought to play a role in molecular communication between the neuron and the glial cell. Thus, multiple roles of the paranodes are crucial for maintaining the normal formation of myelinated nerves.

Disruption of axoglial interaction at the paranodes results in severe pathological conditions in a variety of mouse mutants that are deficient in paranodal and myelin molecules (6–11). All of these so-called *paranodal mutants* lack a normal paranodal junction and display ataxia, motor deficits, and dramatically reduced nerve conduction velocities. Altered paranodal structures have also been reported in human demyelinating diseases such as Charcot-Marie-Tooth disease (CMT), an inherited degenerative neuropathy of the PNS (12, 13), and multiple sclerosis (14, 15).

Mutant phenotypes in mice often closely resemble human disease phenotypes; therefore, these mouse mutations can provide valuable models to understand how the diseases develop and to test ways to prevent or treat the corresponding diseases (16–18). Shambling (gene symbol, *shm*) was originally discovered in the Jackson Laboratory in 1960 and has been propagated in our laboratory for 20 years. Mutant mice exhibit ataxia and motor deficits resulting in hindlimb paresis. Here, we identify the mutated gene and show that it encodes contactin-associated protein, Caspr (also termed *paranodin* or *NCP1*), a major component of the paranode (19–21). This is the first report of a mutation of the *Caspr* gene.

MATERIALS AND METHODS

Animals

Heterozygous shambling mice (SHM-*shm*/+) are maintained at the Research Institute of Environmental Medicine in Nagoya University under approval of the ethics committee

From the Research Institute of Environmental Medicine (XS, YT, YK, SM, KM, MI, YK, YH, YM) and Graduate School of Bioagricultural Science (EO, YC, SO), Nagoya University, Nagoya, Japan; and Department of Molecular Cell Biology (EP), The Weizmann Institute of Science, Rehovot, Israel.

Send correspondence and reprint requests to: Yoshiko Takagishi, PhD, Department of Genetics, Research Institute of Environmental Medicine, Nagoya University, Nagoya 464-8601, Japan; E-mail: taka@riem.nagoya-u.ac.jp

Xiao-yang Sun and Yoshiko Takagishi contributed equally to this work.

This work was supported by a Grant-in-Aid for Scientific Research (20500370), 21st century COE program from the Japan Society for the Promotion of Science and the National Multiple Sclerosis Society (Elior Peles).

Online-only color figures are available at http://www.jneuropath.com.

for animal experiments of the Institute and in accordance with the Guidelines for Animal Experimentation of the Japanese Association for Laboratory Animal Science. Animals are housed in a room at 22°C ± 1°C with a light-dark cycle of 12 hours each. Food and water are given ad libitum. MSM mice, an inbred strain originating from Japanese wild mice (*Mus musculus molossinus*), were also used in the genetic analysis. The MSM mice were supplied by the National Institute of Genetics (Mishima, Japan).

Genetic Mapping

Genomic DNA was prepared from mouse tail tissue by standard phenol-chloroform extraction and ethanol precipitation methods. Fifty nanograms of DNA were subjected to polymerase chain reaction. The primers used for this analysis amplify DNA fragments of different sizes from SHM-*shm*/+ and MSM mice. Primer sequences and allele sizes are available from the Mouse Microsatellite Data Base of Japan (www.shigen.nig.ac.jp/mouse/mmdbj/microsatelliteMapAction.do?chromosome = 11).

The *shm* locus has been mapped to chromosome 11 and has been found to be located 1.5 ± 0.7 cM from the *Re* locus (22). To reduce this region, classical genetic mapping was used. In brief, heterozygous SHM-*shm*/+ mice were crossed with C57BL/6J (B6) inbred mice to generate heterozygous B6-*shm*/+ congenic mice. The genotypes of F2 offspring (total number of mice, 202) were analyzed using microsatellite markers adjacent to the *Re* locus. Because of the low rate of recombination in the original cross, a second cross between SHM-*shm*/+ mice and MSM+/+ mice was also performed (total number of mice, 389).

Reverse Transcription–Polymerase Chain Reaction and Sequencing

Complementary DNA (cDNA) was synthesized from 2 μg of total RNA using the SuperScript III Preamplification System for First Strand cDNA Synthesis (Invitrogen Corp, Carlsbad, CA). Primers to amplify the entire coding regions of the candidate genes were designed using their cDNA sequences in GenBank. Amplified fragments were cloned into pGEM-T easy vector (Promega, Madison, WI) and sequenced using an ABI 373A DNA sequencer (Applied Biosystems, Foster City, CA).

RNA Extraction and Northern Blot Analysis

Total RNAs were extracted from brains of mutant mice and their normal littermates on postnatal day (P) 22 to 28 (n = 3 for each) by the acid-guanidine-phenol-chloroform method (23). Fifteen-microgram aliquots of total RNA were used in the identification of *Caspr* mRNA. The procedures for RNA denaturation, electrophoresis, and hybridization were as previously described (24). *Caspr* cDNA was labeled with [a-32P] dCTP (specific activity, 111TBq/mmol) (PerkinElmer Life and Analytical Sciences, Boston, MA) using a Random Primer DNA labeling Kit Ver. 2 (Takara Bio Inc, Otsu, Japan) and used as a probe. After hybridization, the radioactivity of the band representing *Caspr* mRNA was measured using a Fuji Bioimage Analyzer (BAS 2000; Fuji Photo Film, Tokyo, Japan). The hybridized membrane was reprobed with cDNA for 18S ribosomal RNA as a control.

Western Blot Analysis

Total proteins were extracted from the cerebellum, spinal cord, and sciatic nerves of normal and mutant mice on P22 to P28 (n = 3 for each). Aliquots of 80 μg protein were separated on 7.5% sodium dodecyl sulfate–polyacrylamide gel electrophoresis gels and transferred to a polyvinylidene fluoride membrane (Millipore, Bedford, MA) with Trans-blot SD (Bio-Rad, Hercules, CA). After washing with Tween–Tris-buffered saline, the membranes were incubated with anti-Neurexin/Caspr (BD Biosciences, San Jose, CA) in Can Get Signal® solution I (Toyobo Co Ltd, Osaka, Japan) overnight at 4°C, followed by incubation with anti-mouse horseradish peroxidase–conjugated IgG (Jackson ImmunoResearch, West Grove, PA) in Can Get Signal® solution II for 1 hour. Specific reactivity was visualized with Supersignal® West Pico enhanced chemiluminescence substrate (Pierce, Rockford, IL) and an ATTO cool saver system (Atto, Osaka, Japan).

Electron Microscopy

Normal and mutant mice at P46 to 4 months old (n = 3 for each) were anesthetized with Nembutal and transcardially perfused with 2% paraformaldehyde and 2.5% glutaraldehyde in 0.1 mol/L phosphate buffer. The spinal cord, optic nerves, and sciatic nerves were dissected, and the tissues were cut into small pieces. The tissue pieces were postfixed with 1% OsO_4 in phosphate buffer for 1 hour. After dehydration through graded alcohols, the tissues were embedded in epoxy resin. Semithin sections were cut and stained with toluidine blue for light microscopy. Ultrathin sections were examined with an electron microscope (JEM-1210; JOEL Ltd, Akishima, Japan).

Quantification of Nodal Gaps and Paranodal Loop Gaps

Ultrathin longitudinal sections of the sciatic nerve were examined in 2 sets of mutant and wild-type pairs of mice. Electron micrographs of the node of Ranvier were taken at magnification 5,000× for measurement of the length of the node and at 20,000× to quantify gaps between the axon and glial membrane; the images were scanned and digitized in Photoshop. The gap between the axonal surface and the center of each paranodal loop was measured as a straight line from the outer leaflet of the axon membrane to the outer leaflet of the opposing glial cell membrane. Data from mutant mice and normal littermates were compared statistically using Student *t*-test.

Preparation of Teased Sciatic Nerves and Sections From Optic Nerves and Spinal Cord

Sciatic nerves were removed from mutant and littermate normal mice from P14 to 2 months of age (n = 6 for each, mostly P22–P24). The nerve tissues were treated with collagenase (3.6 mg/mL collagenase Type 1; Wako Inc, Osaka, Japan) for 0.5 to 2.0 hours and then teased apart with fine needles. The teased sciatic nerve fibers were mounted on glass slides and fixed with 4% paraformaldehyde in PBS for

15 to 60 minutes. The nerves were stored in PBS at 4°C until use. For staining with an anti-neurofascin (neurofascin 155 [NF155]) antibody, the nerves were fixed for an additional 15 minutes in Zamboni fixative.

For tissue sections, normal and *shm* mice aged 1 to 2 months (n = 3 for each) were fixed by cardiac perfusion with 4% paraformaldehyde in PBS, and the lumbar spinal cords were removed. The spinal cords were cryoprotected with 30% sucrose and frozen in liquid nitrogen. The tissues were sectioned at 10 to 16 μm on a cryostat.

Immunofluorescence Microscopy

After several washes in PBS, the nerves or tissue sections were permeabilized with 0.3% Triton X-100 in PBS for 30 minutes and blocked in 3% goat serum/5% bovine serum albumin in PBS at room temperature for 1 hour. They were incubated at 4°C overnight with primary antibodies in PBS containing 1% bovine serum albumin. The following antibodies were used: affinity-purified mouse monoclonal and rabbit polyclonal antibodies to Caspr (1:200 and 1:2000) (25, 26); mouse anti-contactin (BD Biosciences); rabbit anti-NF155 (a gift of H. Baba, Tokyo University of Pharmacy and Life Sciences, Tokyo, Japan); rabbit anti-protein 4.1B (Protein Express, Cincinnati, OH); mouse anti-sodium channel (Sigma, St Louis, MO); and rabbit anti-potassium channel (Kv1.1) (Chemicon, Temecula, CA). Nerves were washed for 1 hour at room temperature in PBS before application of Alexa488- or Alexa568-labeled antibodies (Jackson ImmunoResearch). Nerves stained with a fluorescent secondary antibody were washed in PBS, mounted in VECTASHIELD (Vector Lab, Inc, Burlingame, CA), and analyzed with a Zeiss LSM 510 confocal laser scanning microscope (Carl Zeiss MicroImaging, Jena, Germany).

Electrophysiology

Normal and mutant mice aged 2 to 3 months (n = 4 for each) were anesthetized with pentobarbital sodium (50 mg/kg, intraperitoneally). The sciatic nerve along with its continuing tibial nerve was removed, put on an array of Ag-AgCl electrodes, and covered with warmed mineral oil. The distal part of the nerve was stimulated, and the compound action potential (CAP) was recorded at the proximal part. The following stimulus parameters were used: pulse width 10 milliseconds and current intensity at 10% more than the intensity that elicited maximal CAP amplitude. The conduction velocity was determined by the conduction delay between the stimulus artifact to the peak of CAP and the distance (12 mm) between the stimulation cathode and the recording electrode. The temperature of the mineral oil in the recording chamber was measured (range, 28°C–33°C), and the conduction velocity was corrected to that at 37°C (27). The CAPs were amplified, digitized, and analyzed with PowerLab and Scope 3.7 (AD Instruments, Spechbach, Germany).

Visual evoked potential (VEP) recording was carried out in normal and mutant mice aged 3 to 4 months (n = 4 for each) that had been anesthetized with a mixture of fentanyl (0.1 mg/kg) and droperidol (5 mg/kg). The mice were secured onto a stereotaxic instrument, and a small portion of the skull overlying the visual cortex was carefully drilled and removed leaving the dura intact. The VEPs were recorded from the binocular region of the visual cortex (2.7 mm lateral and 3.5 mm posterior to the bregma). The tip of a tungsten microelectrode (FHC Inc, Bowdoinham, ME; 0.5 MΩ) was placed about 500 μm below the cortical surface. The position of the tip was adjusted to achieve the maximal VEP amplitude. Visual stimulation consisted of full-field sine wave gratings of 100% contrast (mean luminance, 25 cd/m^2) at 0.05 cycle per degree was reversed at 1 Hz. Stimuli were generated by a VSG2/5 card (Cambridge Research System, Kent, UK) and presented on a computer monitor. The display was positioned 28.5 cm in front of the mouse and centered on the midline, thereby occupying 60 degrees × 100 degrees of the visual field. Mean luminance was determined by a photodiode placed in front of the computer screen and was 50 cd/m^2. Electrical signals were amplified and filtered (high-pass filter, 0.01 Hz; low-pass filter, 1 kHz). The VEP amplitude was determined by the average for 150 stimuli presented to the eye contralateral to the recorded hemisphere.

RESULTS

Neurological Phenotype of Shambling Mice

Shambling mutant (*shm/shm)* mice were easily distinguished from their normal littermates by their smaller size and wobbly gait caused by hindlimb weakness. The abnormal locomotion was first noted around P14 to P15 by slow motor activity and lack of coordination in hindlimb movement. After 3 weeks, the body sizes of the mutant mice barely increased. An ataxic gait and trembling body were also noticeable by 3 weeks of age. The mutant mice adopted an abnormal posture in which their hindlimbs extended laterally, which worsened with age so that their hindlimbs were held stiffly up and off the cage floor (Fig. 1A). The motor deficit was also progressive, and occasionally the mice became immobile as they aged. Many mutant mice died around weaning and special care measures such that reducing the number of pups in the litter and giving them ground food were required to aid their survival beyond weaning.

Identification of the Gene Responsible for the *shm* Phenotype

To identify the gene mutation responsible for the *shm* phenotype, we performed positional cloning using microsatellite DNA markers. Analysis of the F_2 offspring from an initial cross of SHM-*shm*/+ and B6 mice indicated that the *shm* gene was localized within a 4.5-megabase (Mb) interval between markers D11Mit58 and D11Mit59. To further narrow this region, we used a second cross between SHM-*shm*/+ and MSM+/+ mice. Analysis of 389 F_2 mice from this cross-localized *shm* to an interval of 0.24 Mb between D11Oda21 and D11Oda27; we developed these as new microsatellite DNA markers (Fig. 1B).

From the mouse genome databases, 17 genes were identified in this 0.24-Mb region (Fig. 1C). We selected 14 of these, amplified their cDNAs in brain tissues from mutant and normal mice, and sequenced the resulting cDNAs. We found a TT insertion in exon 22 of the contactin-associated protein (*Caspr*) gene (Fig. 1D). *Caspr* maps at 100.8 Mb on

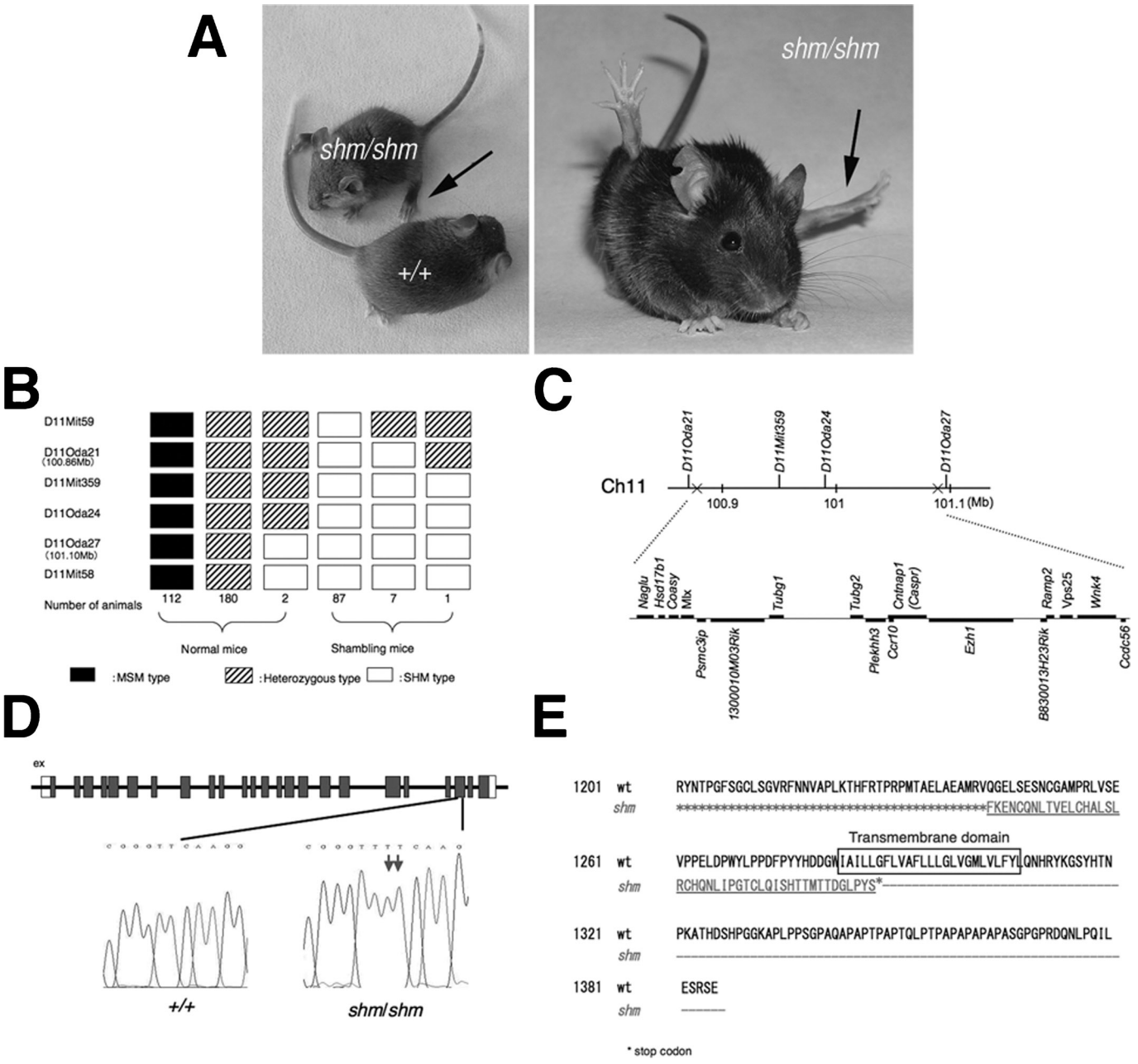

FIGURE 1. Identification of the *Caspr* gene in shambling mice. **(A)** Phenotypes of shambling mice. Left: Normal (+/+) and mutant (*shm/shm*) littermates at P21. Right: 4-month-old mutant mouse. The arrow indicates a stiff and extended hindlimb (left) and the characteristic hindlimb paresis (right). **(B)** Haplotype recombination frequencies in F2 offspring (SHM+/*shm* × MSM+/+) localize the mutated gene to the region between microsatellite DNA markers D11Oda21 and D11Oda27. **(C)** Schematic diagram of the mutant locus. Upper: Physical map of the polymorphic markers between D11Oda21 and D11Oda27. Lower: Schematic diagram of the genes present in the region between the 2 DNA markers. **(D)** The mutation in the *Caspr* gene of *shm* mice. A TT insertion (double arrows) has occurred in exon 22. **(E)** Partial alignment of the deduced amino acid sequences of the wild-type (wt) Caspr protein and the truncated (*shm*) protein.

chromosome 11. The gene contains 24 exons and a 4,158-bp open reading frame encoding 1,385 amino acids. The TT insertion caused a frame shift resulting in an altered sequence of 45 amino acid residues at the C terminus. In addition, the insertion generated a stop codon at amino acid residue 1287 of the protein so that 98 amino acid residues were deleted from the C terminus of the mutated Caspr protein. The deleted region contained the transmembrane and cytoplasmic

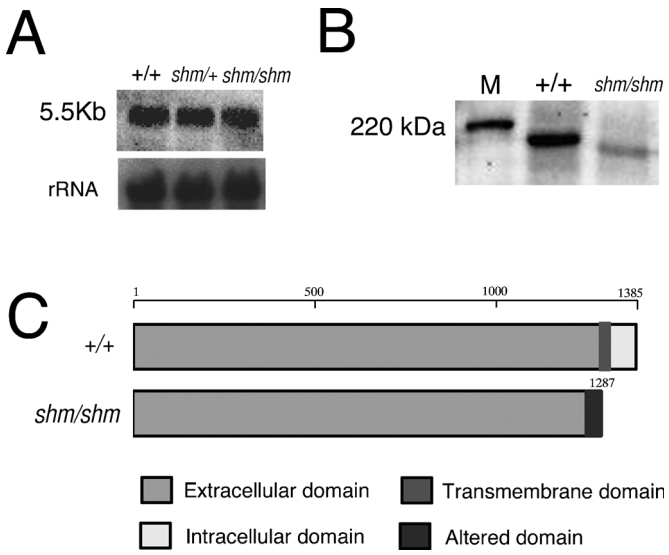

FIGURE 2. Expression of *Caspr* mRNA and protein in the cerebellum. **(A)** Northern blot analysis. There are no differences among the sizes of the RNAs from wild-type (+/+), heterozygous (*shm/+*), and homozygous (*shm/shm*) mice. **(B)** Western blot analysis. There is a band with a molecular mass of 190 kd in wild-type mice (+/+) and a smaller band with the expression level reduced in the mutant (*shm/shm*) mice. **(C)** Schematic representation of the Caspr protein in normal (+/+) and mutant (*shm/shm*) mice. The mutant protein is expected to lack the transmembrane and intracellular domains.

domains of the normal Caspr protein (Figs. 1E, 2C). Moreover, an analysis using TMHNN severe 2.0 (www.cbs.dtu.dk/services/TMHMM-2.0/) indicated that the sequence of the modified region of the mutated protein did not contain transmembrane helices. Thus, it is highly likely that the *shm* mutation in the *Caspr* gene generated a protein that lacks the transmembrane and cytoplasmic domains.

Expression of Caspr mRNA and Protein in the *shm* Mice

Next, we examined whether expression of *Caspr* mRNA and protein was affected in the brains of *shm* mutant mice. Northern blot analysis detected a 5.5-Kb band for *Caspr* mRNA in brains of both normal and *shm* mice, and their expression levels were similar (Fig. 2A).

Expression of the Caspr protein was examined by Western blot using antibodies against the extracellular domain of Caspr. The Caspr protein was detected as a single band of the expected molecular mass of 190 kd in the normal cerebellum, but in the *shm* cerebellum, a smaller and weaker band was present (Fig. 2B). The same results were obtained for the spinal cord and sciatic nerves (data not shown). These data indicate that a truncated Caspr protein was produced as expected, and that its expression level was decreased in the *shm* CNS and PNS.

Morphological Analysis

Light microscopy of sciatic nerves and the white matter of the spinal cord revealed that the numbers of myelinated axons, thickness of the myelin sheath, and diameter of the axons were similar in normal and mutant mice (Figs. 3A–D). We did not attempt to quantify these characteristics.

By electron microscopy, sciatic nerves, node, and paranodes appeared to form normally in *shm* mice, but the axonal cytoplasm occasionally contained abnormally large mitochondria and showed accumulation of mitochondria and other organelles at the nodal and paranodal regions (Figs. 3E–H). Furthermore, the lengths of the node were longer in *shm* mice than in normal mice (1,625.2 ± 163.5 nm, n = 6 vs 1,091.6 ± 55.2 nm, n = 4; $p < 0.05$), indicating that the nodes were widened in the mutant mice.

At the highest magnification used, myelin loops were arrayed sequentially and in close apposition to the axonal membrane in normal paranodes in *shm* mice (Figs. 4A, C). The periodic transverse dense bands were present between the loops and the axonal membrane, termed the *paranodal junctions* (Figs. 4A, C). In contrast, paranodal junctions were absent from the paranodes of *shm* sciatic nerves, although paranodal loops faced the axolemma and compact myelin formation appeared normal (Fig. 4B). Measurement of the space (gap) between paranodal loops and the axonal plasma membrane indicated that the gaps in mutant mice were significantly wider than those in normal mice (13.12 ± 1.11 nm, n = 18 vs 5.97 ± 0.37, n = 9; $p < 0.001$).

In the CNS paranodes of *shm* mice, in addition to the absence of the paranodal junctions (Fig. 4D), the loops faced away from the axonal membrane and were frequently everted (Fig. 4E). Occasionally, the loops were layered over the everted loops (Fig. 4E). Electron-dense material was occasionally present between myelin loops and axolemma at the paranodes (Fig. 4D). Together, these data indicate that the axoglial junctions are disrupted at the paranodes of *shm* mutant mice.

The localization and distribution of proteins at the paranodal regions including the node and juxtaparanode were investigated next. We first determined whether the mutant Caspr protein was located to the paranode of *shm* mice by performing an immunohistochemical analysis of sciatic nerves using different anti-Caspr antibodies. The antibody that recognizes the cytoplasmic domain of Caspr (R6061) did not stain the paranodal regions of *shm* sciatic nerves, whereas staining was present at the paranode when an antibody directed to the extracellular domain of Caspr (M275) was used (Fig. 5A). The intensity of Caspr staining varied among the paranodes in *shm* sciatic nerves, however. In addition to the normal profile expected of Caspr staining (Figs. 5A, Ba), some paranodal regions showed faint and diffuse staining with the Caspr antibody (Fig. 5Bb). Caspr staining was not often encountered at the paranodal region of *shm* sciatic nerves (Fig. 5Bc). These observations are consistent with the Western blot analysis in which Caspr protein expression was decreased in the mutant mice.

To assess how often Caspr staining was present at the paranodal regions of *shm* myelinated nerves, we performed doubling staining with anti-Caspr and anti-Kv1.1 antibodies. The anti-Kv1.1 antibody stained K^+ channels at the juxtaparanode in normal myelinated nerves and at the paranode in *shm* myelinated nerves. We quantified the frequencies of the

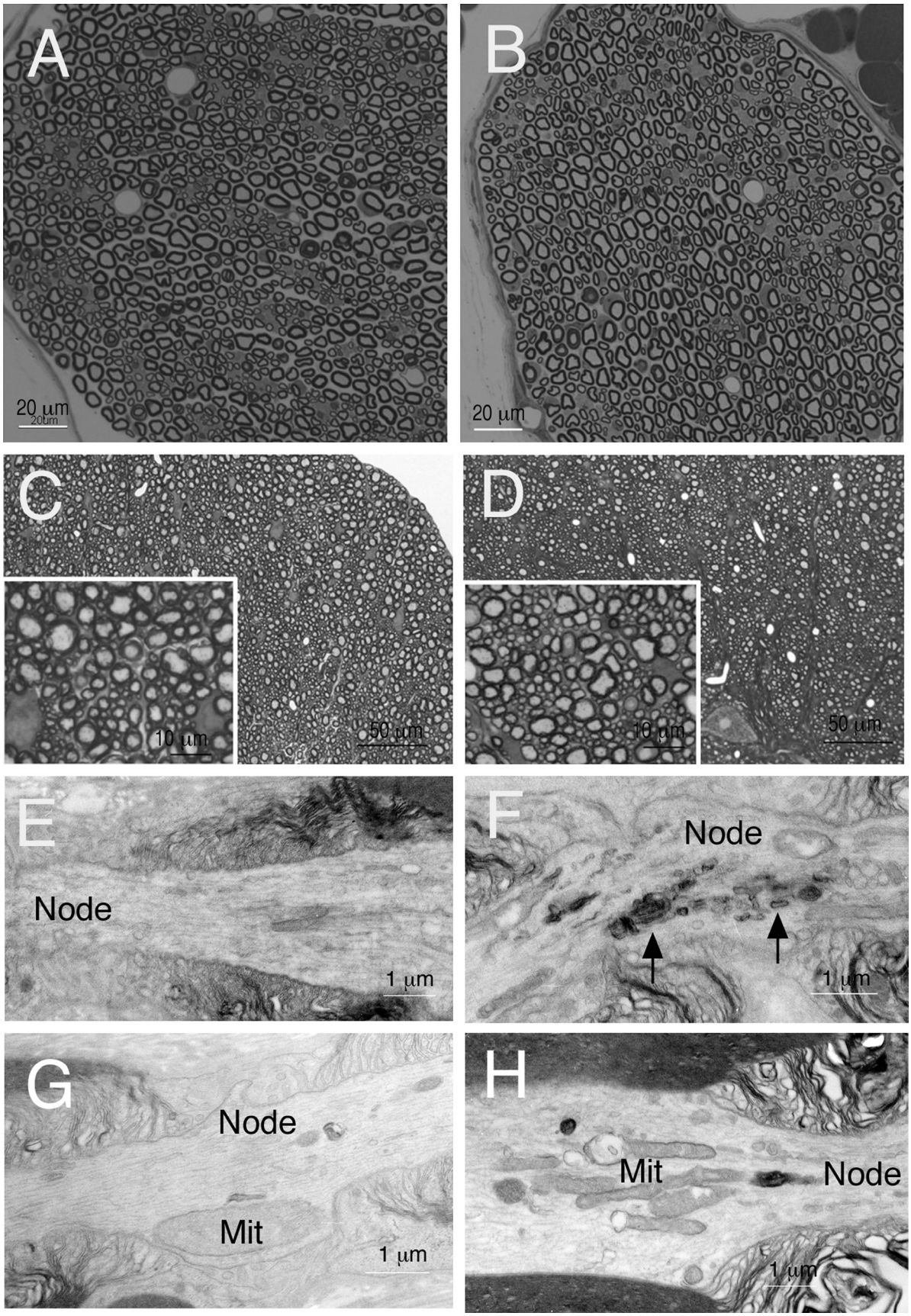

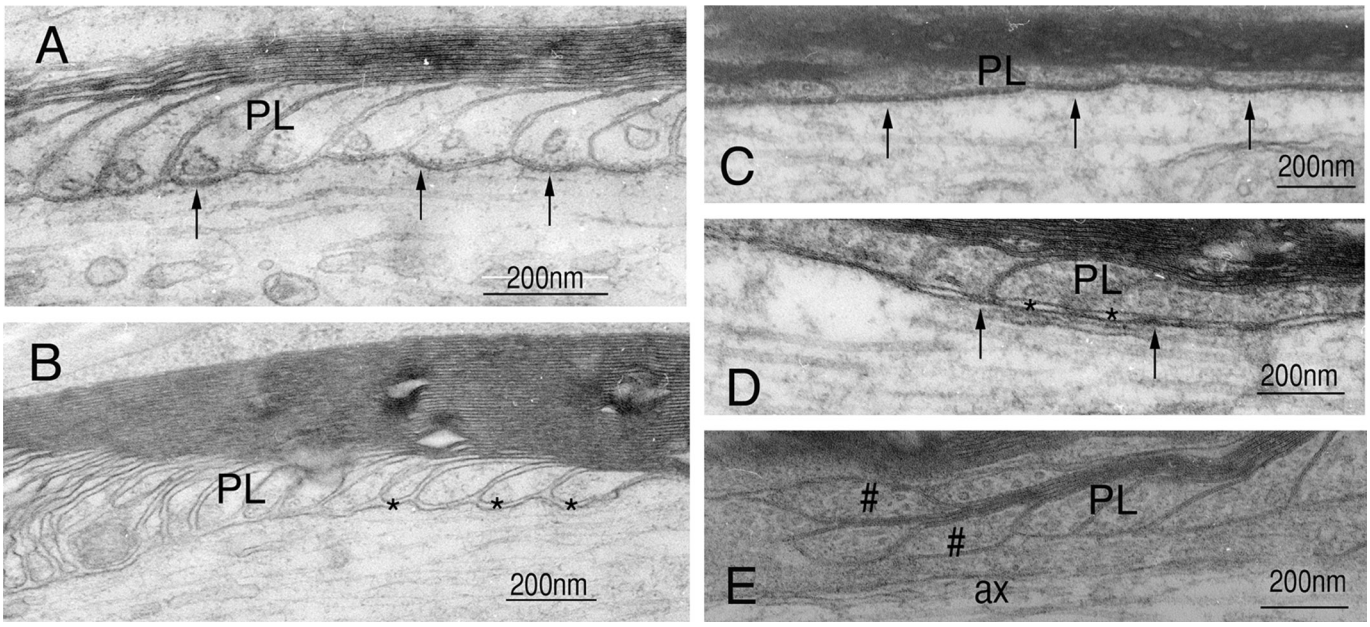

FIGURE 4. Ultrastructure of paranodes in normal and shambling mice. **(A, B)** Sciatic nerves from normal **(A)** and *shm* mutant mice **(B)**. **(C–E)** Optic nerves from normal **(C)** and *shm* mutant mice **(D, E)**. In normal paranodes, paranodal loops (PL) are arrayed sequentially in close apposition to the axonal membrane **(A, C)**. The periodic dense transverse bands are present between loops and axonal membrane (arrows). In contrast, in mutant paranodes, these bands are absent (asterisks in **[B]** and **[D]**). In optic nerves, however, electron-dense material is present in some regions (arrows in **[D]**); the loops also face away from the axolemma (ax) and are everted (#). **(A)** P53; **(B)** P52; **(C–E)** P40.

paranodal staining profiles, including nodes and juxtaparanodes, and classified them as having or lacking Caspr staining; 24.19% ± 9.19% (mean ± SEM, n = 3, P22 mice) of the paranodal regions showed Caspr staining (Figs. 5C, D). Thus, *shm* Caspr was present in the paranodal region of approximately one quarter of the sciatic nerves, although there was variation in the staining pattern (Figs. 5Ba, Bb). The remainder of the paranodes lacked Caspr, presumably as a result of generation of the mutant Caspr protein. Because the *shm* Caspr lacks transmembrane and cytoplasmic domains (Fig. 2C), it could not form a stable association at the plasma membrane (28). An alternative explanation is that the mutant Caspr is transported less efficiently to the axon from the soma. We found that the extracellular domain of the *shm* Caspr protein is intact. Normally, the extracellular domain of Caspr interacts with contactin, and this interaction is essential for the axonal transport of Caspr (29, 30).

To investigate this issue, we examined spinal cord neurons to determine whether Caspr was retained in the soma. In normal mice, Caspr staining was observed at the paranode within the white matter of the lumbar spinal cord. By contrast, staining was weaker in the white matter in mutant mice compared with normal mice. The mutant mice occasionally showed staining that was confined to the neuronal soma in the ventral horn (Fig. 5E). These findings suggest that the mutated Caspr was synthesized in the soma of motor neurons but was only partially transported to the axon.

To determine whether the truncated Caspr protein of the *shm* mutant affects the organization of paranodal components, we examined expression and localization of paranodal proteins by immunohistochemistry in *shm* sciatic nerves. Contactin is a glycosyl phosphatidylinositol–anchored IgSF cell adhesion molecule (31). Caspr and contactin form an adhesion complex that is essential for the formation of the paranodal junction (7, 32). In normal sciatic nerves, contactin immunostaining was restricted to the paranode (Fig. 6A). In *shm* sciatic nerves, however, contactin displayed a range of staining patterns, but the normal paranodal profile was rarely detected (Fig. 6A). These results are similar to those obtained for Caspr. Therefore, we counted the number of paranodal profiles with and without contactin staining by double labeling with anti-Kv1.1 antibodies and found that 52.84% ± 10.11% (mean ± SEM, n = 3, P22–24 mice) of paranodal regions showed contactin staining (Fig. 6B). As for Caspr, contactin immunoreactivity in

FIGURE 3. Histology of myelinated nerves in normal and shambling mice. **(A–D)** Cross sections of sciatic nerves from normal **(A)** and *shm* mutant mice **(B)** and of the ventral regions of the spinal cords of normal **(C)** and *shm* mutant mice **(D)**. Insets show higher magnification images. There are no obvious differences in axon or compact myelin formation between normal and mutant mice. Plastic-embedded sections stained with toluidine blue. **(E–H)** Electron micrographs of sciatic nerves from normal **(E)** and *shm* mutant mice **(F–H)**. The axoplasma of normal myelinated nerves are enriched in tubular and filament organelles **(E)**. In the mutant mice, there are abnormal organelles (i.e. aggregated lysosomes) (**[F]** arrows) and swollen mitochondria (Mit) **(G)** in the nodes. Mitochondria are also abundant in the paranodal region **(H)**. **(A–D)** P50; **(E)** 4 months; **(F–H)** P50.

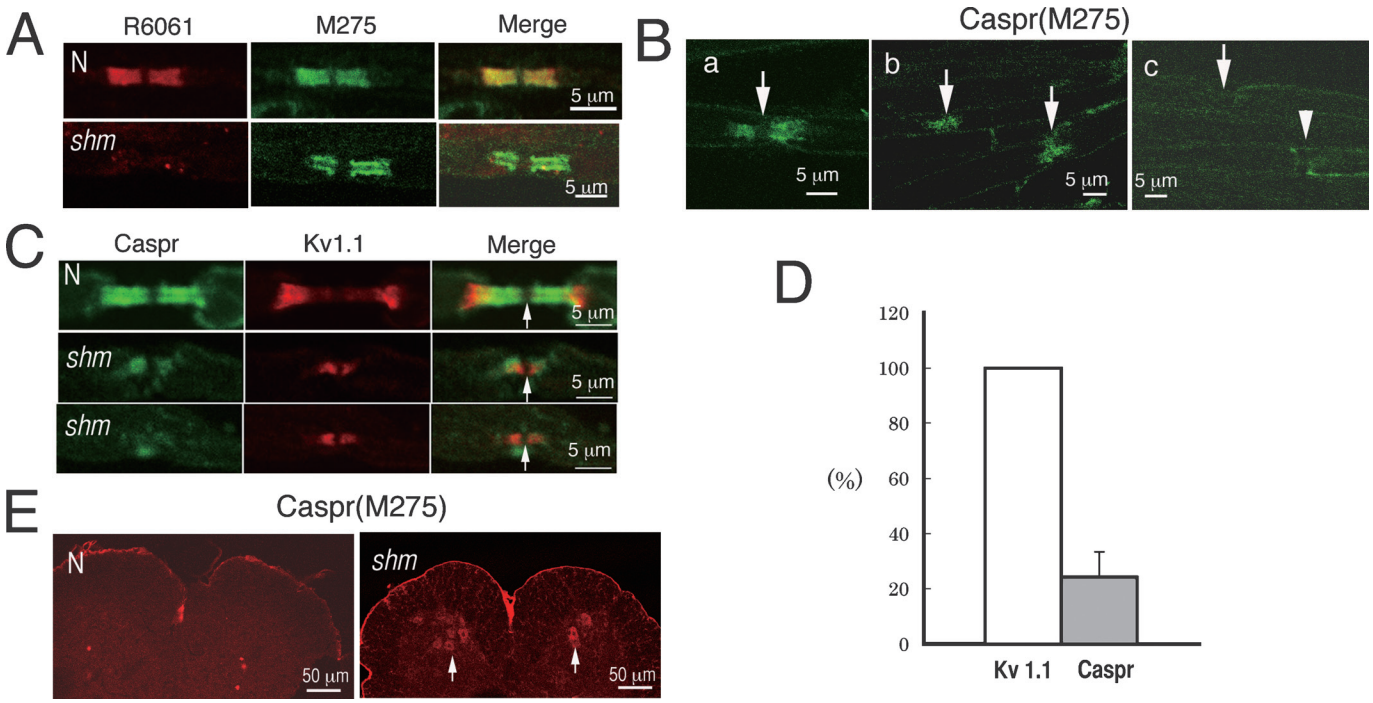

FIGURE 5. Expression and localization of the Caspr protein. **(A–D)** Sciatic nerves. **(E)** Spinal cords. **(A)** Caspr staining is not detected in *shm* mutant mice using an antibody against the cytoplasmic domains (R6061), but an antibody against the extracellular domain (M275) stains the paranodes of mutant mice. **(B)** The distribution pattern of Caspr at the paranodal region in *shm* mice. Arrows indicate the node. An arrowhead indicates Schmidt-Lanterman incisures. **(C)** Double labeling of Caspr (green) with Kv1.1 (red) for identification of paranodal profiles. Arrows indicate the node. **(D)** Percentage (%) of Caspr staining at paranodal regions after staining using anti-Kv1.1 antibody. Paranodal profiles were analyzed from 3 normal and 3 *shm* mice (100 each). **(E)** No cells in the ventral horn of a normal mouse are stained (left); large motor neurons express Caspr in an *shm* mutant mouse (arrows in right panel). **(A)** P24 to 30; **(B)** P14 to P24; **(C)** P22 to P24; **(E)** P30.

lumbar spinal cord neurons of *shm* mice was also retained in the somata (data not shown).

Neurofascin 155 is a cell adhesion molecule expressed on the glial surface on the opposing paranodal loop (11, 33). It is believed that a complex of Caspr and contactin binds to NF155 at paranodes (33, 34). Neurofascin 155 staining was detected at the paranodal region; however, the immunoreactivity was extremely low compared with that of Caspr and contactin (Fig. 6C). Nevertheless, where NF155 staining was associated with Caspr staining (i.e. where Caspr was concentrated in the paranodal regions), NF155 was also present; and where Caspr was minimal, NF155 was also less evident.

The cytoplasmic domain of the normal Caspr protein interacts with protein 4.1B, providing a potential link with the actin cytoskeleton. This interaction is necessary to anchor a Caspr-contactin complex to the axonal membrane (28). Immunostaining for protein 4.1B revealed that it was expressed and distributed normally at the paranodes in *shm* sciatic nerves. Double staining for protein 4.1B and Caspr showed that protein 4.1B staining was apparently normal even when Caspr staining was barely detectable in the paranodal region (Fig. 6D).

We next examined whether altered distribution of paranodal molecules affected localization of the voltage-gated channels. The Na^+ channels at the node and the K^+ channels at the juxtaparanode are functionally crucial for generating action potentials and for propagating saltatory conduction. In the double staining for Na^+ channels and K^+ channels (Kv1.1) in normal axons, both were separated at each domain by a paranodal junction (Fig. 7A). In *shm* mutant mice, Na^+ channels and K^+ channels were closely located (Fig. 7B). The Na^+ channels were restricted to the node, whereas the K^+ channels were adjacent to the nodes (Fig. 7C). Thus, the K^+ channels were mislocalized at the paranode in *shm* sciatic nerves.

Electrophysiological Analysis of Sciatic Nerves and Optic Nerves

We investigated whether disruption of the paranodal junction and the altered distribution of ion channels affected conduction of nerve impulses in *shm* mutant mice. Nerve conduction velocity was assessed by measuring CAPs in sciatic nerves isolated from normal and mutant mice. The electrophysiological properties of the sciatic nerves in the genotypes are summarized in the Table, and the differences in CAP waveforms are illustrated in Figure 8A. The CAPs of mutant mice exhibited markedly reduced peak-to-peak amplitude and delayed onset compared with those of normal mice. The mean conduction velocity in mutant mice was significantly reduced to 45.1% of that of normal mice ($p < 0.0001$; Table). Similarly, the reduction in CAP peak-to-peak amplitudes

was statistically significant (Table). The minimum voltage threshold required to elicit a CAP was also significantly higher

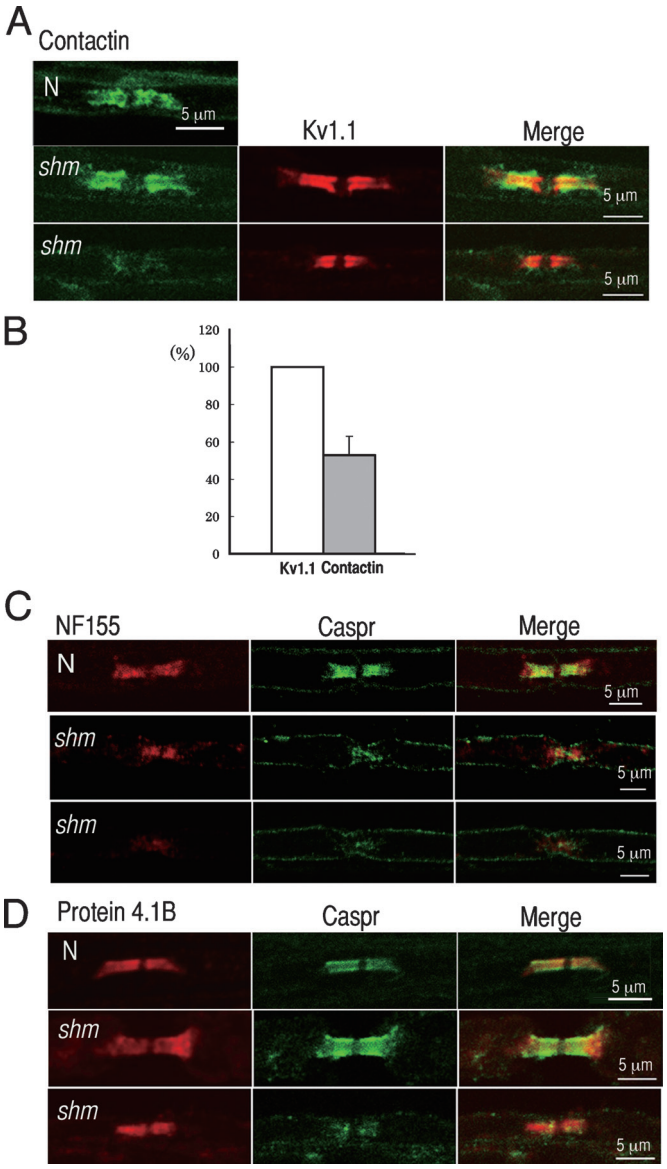

FIGURE 6. Expression of paranodal proteins in sciatic nerves. **(A)** Contactin. Double staining for contactin (green) and Kv1.1 (red) shows intimate and discrete expression of contactin at the paranodes in an *shm* mutant mouse. **(B)** Percentage (%) of paranodes with contactin and Kv1.1 staining. Paranodal profiles were counted from 3 normal and 3 *shm* mice (100 each). **(C)** NF155. NF155 (red) and Caspr (green) staining. The pattern of NF155 staining is similar to that of contactin in *shm* mice. There is faint Caspr staining on the outer surface of the myelinated nerves in both normal (N) and *shm* mice. Staining of the basement membrane appears to be nonspecific because of the use of a mouse monoclonal antibody. **(D)** Protein 4.1B. Double staining for protein 4.1B (red) and Caspr (green) shows that Protein 4.1B is distributed independently of Caspr at the paranodes. Nerves are from normal and *shm* mice at P22 to P30.

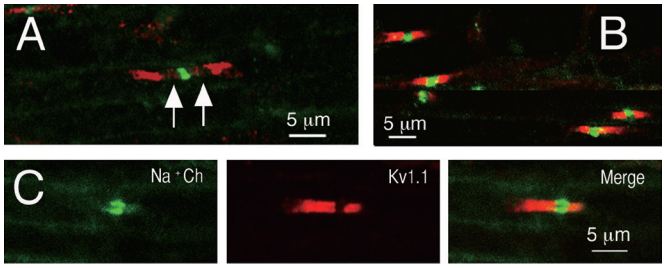

FIGURE 7. Distribution of voltage-gated channels at the paranodes in sciatic nerves from normal and *shm* mice at P22 to P24. In normal mice **(A)**, Na^+ channels (green) are located at the node of Ranvier and the K^+ channels (Kv1.1, red) at the juxtaparanode; they are separated by intervening paranodes (arrows). In *shm* mice **(B)**, the channels are adjacent, indicating that the K^+ channels are mislocalized at the paranodes **(C)**.

in mutant mice than normal mice (Table). Overall, therefore, these data indicate that saltatory conduction in sciatic nerves in *shm* mice is impaired because of the disruption of the paranodal junctions and altered distribution of ion channels.

We also recorded VEPs from the primary visual cortex of *shm* and normal mice. The VEPs elicited in the mutant mice in response to contralateral eye stimulation were far smaller than those of normal mice (Figs. 8B, C). The mean amplitude of VEPs was significantly smaller ($p < 0.01$) in mutant mice than control mice (Fig. 8D). Likewise, the latency of VEPs was significantly longer ($p < 0.04$) in mutant mice than normal mice (Fig. 8E). Thus, the data indicate that the pathway to the primary visual cortex was severely affected in *shm* mutant mice.

DISCUSSION

Caspr Mutation in *shm* Mice

The *shm* mouse was identified in the fifth generation of mice after spermatogonial X-irradiation (35). Although it was discovered more than 4 decades ago, however, the responsible gene had not been identified nor had its pathogenesis been investigated in depth before this study. To date, no *Caspr* gene mutations have been reported in rodents or humans. We found that a TT insertion in exon 22 resulted in a stop codon in exon 23 of the *Caspr* gene of *shm* mice (Fig. 1D). The *shm* mutation apparently escaped from

TABLE. Electrophysiological Analysis of Sciatic Nerves

Mice	CV, Meters per Second	Threshold, V	PkAmp, mV	No. Samples in Group
Wild type +/+	30.6 ± 0.7	0.6 ± 0.1	1.6 ± 0.2	4
shm/shm	13.8 ± 1.2*	2.4 ± 0.2**	0.6 ± 0.1**	4

Measurements are expressed as mean ± SEM.
*$p < 0.0001$, **$p < 0.001$, by Student *t*-test.
CV, conduction velocity; PkAmp, peak-to-peak amplitude.

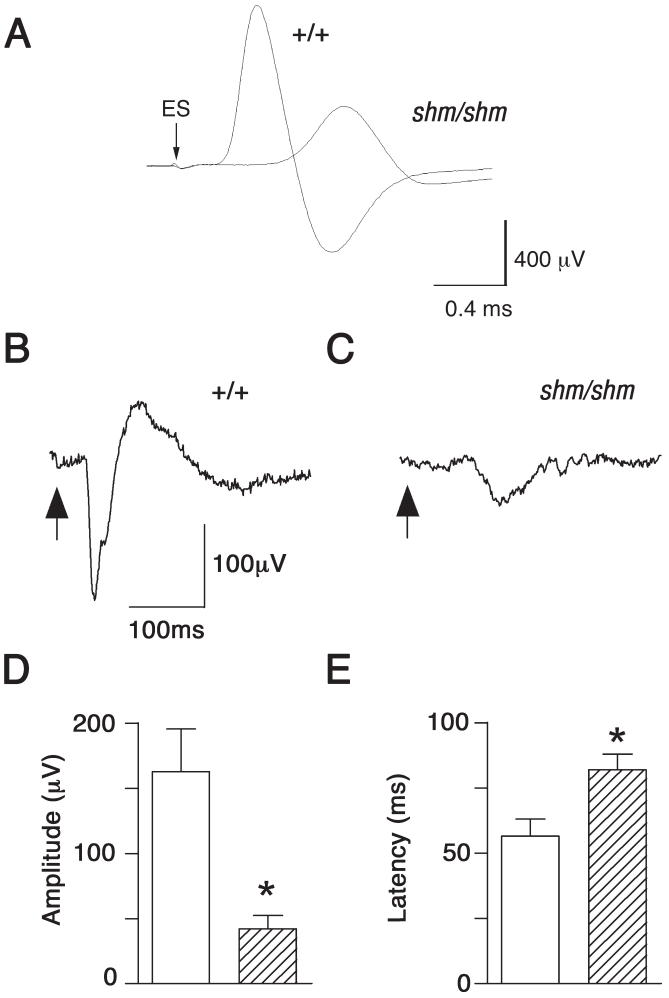

FIGURE 8. Electrophysiological analysis. **(A)** Averaged waveforms of the compound action potential (CAP) recorded from the sciatic nerves of normal (+/+) and mutant (*shm/shm*) mice aged 2 to 3 months. The CAPs are delayed, and the peak-to-peak amplitude is markedly reduced in mutant mice. **(B–E)** Measurement of visual evoked potentials (VEPs) from normal (+/+) and mutant (*shm/shm*) mice aged 3 to 4 months. **(B, C)** Representative average traces of VEPs (n = 150). Mean amplitudes **(D)** and latencies **(E)** of VEPs in normal (open bars) and mutant (shaded bars) mice. n = 4, * $p < 0.05$ (Mann-Whitney U test).

nonsense-mediated mRNA decay as the premature termination codon is located less than 55 bp from an exon-exon interaction in the second exon (36, 37). A truncated Caspr protein lacking the transmembrane and cytoplasmic domains was generated, and expression of the abnormal protein was low in *shm* mice (Fig. 2B). The *shm* mice therefore provide a unique model for investigating the role(s) of the extracellular domain and the cytoplasmic domain of the Caspr protein in the formation and function of paranodal junctions. Thus, we investigated whether a normal paranodal complex was organized and a normal paranodal junction structure was formed in myelinated nerves of *shm* mice.

Expression of the Truncated *Caspr* Protein

The extracellular domain of the Caspr protein binds laterally to contactin; this association is required for the intracellular transport of Caspr from the endoplasmic reticulum and for targeting the protein to the cell surface at the paranode (29, 30). In addition, the cytoplasmic domain of the Caspr protein is necessary for retention of the Caspr-contactin complex at the paranodal junction (28). Because the extracellular domain of the mutated Caspr protein is intact, we anticipated that a Caspr-contactin complex would be inserted into the plasma membrane at the paranode. It was also likely that the truncated Caspr protein would not be capable of being immobilized on the paranodal axolemma and would be internalized in the axon at the paranodal region. Our analysis of *shm* mice revealed a variety of distribution patterns for the mutated Caspr protein: a certain amount of the protein was retained in the soma of motor neurons in the ventral horn of the spinal cord (Fig. 5E), whereas it was also clearly located in some paranodes and adjacent to the paranodes (Figs. 5B, C; 6C, D). Our observations indicate that the axonal transport of Caspr is somewhat aberrant in *shm* mutant mice. Because there was a faint diffuse staining in the paranodal region (Fig. 5B), some of the truncated Caspr protein might also be internalized within the axon. We suspect that the mutated Caspr protein cannot form a normal paranodal complex in myelinated nerves. Indeed, we observed that paranodal junctions were absent from the sciatic nerves of *shm* mice (Fig. 4B).

The patterns of immunolocalization of contactin and NF155 were similar to that of Caspr at the paranode in *shm* myelinated nerves (Figs. 6A, C). This suggests that *shm* Caspr affected expression and distribution of contactin and NF155. Normally, Caspr is stabilized at the paranode by binding to the axonal cytoskeleton-associated protein 4.1B (1, 2). Our data suggest that the *shm* Caspr did not affect distribution of protein 4.1B at the paranode (Fig. 6D). Mislocalization of protein 4.1B, which is normally distributed along the peripheral myelinated axons, has been reported in *contactin* knockout (KO) (28) and *CGT* KO (38) mice.

In summary, the mutated Caspr protein in *shm* mice was expressed and distributed at the paranode, although the amounts of protein were significantly reduced. In addition, the aberrant expression and distribution of the truncated Caspr influenced paranodal organization because the expression and distribution of other paranodal molecules were also reduced in this region.

Disruption of Paranodal Junctions in *shm* Myelinated Nerves

The most prominent defects of paranodes in *shm* mice were disruption to the paranodal junctions; in particular, the absence of transverse bands and widened gaps between the axonal membrane and paranodal loops. The disruption to paranodal junctions differed between the CNS and the PNS. In the CNS, electron-dense materials were occasionally present, indicating residual material from the paranodal junctions, and myelin loops were more disorganized, with the loops facing away from the axon (everted loops) (Fig. 4).

These findings are consistent with those from *Caspr* KO mice (6). Absence of transverse bands at the paranodal junctions have also been reported in the PNS of *contactin* KO (7), *NF155* KO (11), and *CGT* KO (8) mice.

The disruption to the paranodal junctions in *shm* mutant mice caused the aberrant distribution of voltage-gated ion channels, that is, the Na^+ and K^+ channels. The Na^+ channels were more diffuse at the node: we found that the nodal region was significantly wider and the stained Na^+ channels at the node were longer. Preliminary results from a normal P21 mouse gave a mean length for Na^+ channels of 1.35 ± 0.04 μm ($n = 74$) and from a mutant P21 mouse a mean of 1.80 ± 0.05 μm ($n = 114$). The K^+ channels, which are normally distributed in the juxtaparanode, were mislocated to the paranodal region next to the Na^+ channels at the node in mutant mice (Fig. 7). The paranodal junctions provide a barrier for segregation of Na^+ channels and K^+ channels, which is crucial for producing action potentials for conduction velocity in myelinated nerves (1, 2, 5). The disruption of this barrier may be responsible for the aberrant nerve conduction in *shm* mutant mice. Mislocalization of K^+ channels was also found in *Caspr* KO (6) and *contactin* KO (7) mice.

Aberrant Nerve Impulse Conduction in *shm* Mice

Rapid impulse propagation via saltatory conduction in myelinated nerves is critically dependent on the insulating function of myelin. In the *shm* sciatic nerve, the conduction velocity and the peak-to-peak amplitudes of compound action potentials were markedly reduced possibly caused by disrupted paranodal junctions. In *shm* myelinated nerves, there were no distinct differences in either myelin formation in the axons or the ratio of fiber diameter to myelin thickness (Figs. 3A–D). Reduction of conduction velocity has also been reported in *Caspr* KO (6) and *contactin* KO (7) mice. Aberrant nerve impulse conduction in peripheral nerves likely contributes to the hindlimb weakness commonly displayed by these mice.

We also found that the visual pathway was affected in *shm* mutant mice. The smaller amplitude of VEPs was probably caused by disruption of the axoglial interaction at the paranode (Fig. 4D). Furthermore, the disruption of axoglial interaction at the paranodes may also affect the conduction velocity in optic nerves because the latency of VEPs was prolonged in mutant mice. This is the first report of a defect of nerve impulse conduction in the CNS in mice with a deficiency for paranodal molecules. The VEPs are widely used to assess the function of the visual pathways in both health and disease (39, 40). In *shm* mutant mice, the amplitude of VEPs was very small compared with those in normal mice, indicating that visual function was severely affected. In hypomyelinated *shiverer* mutant mice, a significant increase in latency has also been observed, but there is no consistent difference in the amplitudes of the main peak of the VEPs (41). The small amplitude of VEPs in mutant mice may be ascribed to the conduction failure of nerve fibers mediating visual signals from the retina to primary visual cortex in addition to the prolonged conduction velocity. In summary, a failure to segregate Na^+ and K^+ channels at the nodes and juxtaparanodes caused by disruption of paranodal axoglial junction and altered expression of paranodal proteins is accompanied by aberrant nerve conduction in the PNS and the CNS. These abnormalities likely contribute to the neurological phenotype of *shm* mutant mice.

An Animal Model for Axodegenerative and Possibly Demyelinating Disease

The nodal/paranodal axoplasm of *shm* mice had abnormally large mitochondria and accumulation of cytoplasmic organelles (Figs. 3F–H), suggesting that axonal transport is affected in the nerves. Altered neuron-glial interaction at the paranodes has been reported in human demyelinating diseases such as CMT and multiple sclerosis. The CMT phenotype can be produced by more than 30 different mutations, but to date, there is no evidence that *Caspr* can cause CMT (42). In CMT, however, the paranodal junction is absent and the structure of the node of Ranvier is altered (13), implying that loss of the interaction between glial cells and neurons results in demyelination and axonal degeneration (12). Multiple sclerosis is characterized by the presence of multiple chronically demyelinated lesions and axonal loss, and immunolocalization of Caspr and nodal/juxtaparanodal proteins is diffuse along the axons and not concentrated in these regions (14, 15), suggesting that aberrant location of Caspr may be an early indicator of impending myelin loss in multiple sclerosis. Taken together, we propose that a neurological mutant mouse, shambling, which is a newly identified mutation of *Caspr*, could be a useful animal model for human axodegenerative and possibly demyelinating diseases.

REFERENCES

1. Girault JA, Peles E. Development of nodes of Ranvier. Curr Opin Neurobiol 2002;12:476–85
2. Poliak S, Peles E. The local differentiation of myelinated axons at nodes of Ranvier. Nat Rev Neurosci 2003;4:968–80
3. Sherman DL, Brophy PJ. Mechanisms of axon ensheathment and myelin growth. Nat Rev Neurosci 2005;6:683–90
4. Corfas G, Velardez MO, Ko CP, et al. Mechanisms and roles of axon–Schwann cell interactions. J Neurosci 2004;24:9250–60
5. Peles E, Salzer JL. Molecular domains of myelinated axons. Curr Opin Neurobiol 2000;10:558–65
6. Bhat MA, Rios JC, Lu Y, et al. Axon-glia interactions and the domain organization of myelinated axons requires neurexin IV/Caspr/Paranodin. Neuron 2001;30:369–83
7. Boyle ME, Berglund EO, Murai KK, et al. Contactin orchestrates assembly of the septate-like junctions at the paranode in myelinated peripheral nerve. Neuron 2001;30:385–97
8. Dupree JL, Coetzee T, Blight A, et al. Myelin galactolipids are essential for proper node of Ranvier formation in the CNS. J Neurosci 1998;18:1642–49
9. Dupree JL, Girault JA, Popko B. Axo-glial interactions regulate the localization of axonal paranodal proteins. J Cell Biol 1999;147:1145–52
10. Ishibashi T, Dupree JL, Ikenaka K, et al. A myelin galactolipid, sulfatide, is essential for maintenance of ion channels on myelinated axon but not essential for initial cluster formation. J Neurosci 2002;22:6507–14
11. Sherman DL, Tait S, Melrose S, et al. Neurofascins are required to establish axonal domains for saltatory conduction. Neuron 2005;48:737–42
12. Sahenk Z. Abnormal Schwann cell–axon interactions in CMT neuropathies. The effects of mutant Schwann cells on the axonal cytoskeleton and regeneration-associated myelination. Ann N Y Acad Sci 1999;883:415–26

13. Sahenk Z, Mendell JR. Alterations in nodes of Ranvier and Schmidt-Lanterman incisures in Charcot-Marie-Tooth neuropathies. Ann N Y Acad Sci 1999;883:508–12
14. Wolswijk G, Balesar R. Changes in the expression and localization of the paranodal protein Caspr on axons in chronic multiple sclerosis. Brain 2003;126:1638–49
15. Coman I, Aigrot MS, Seilhean D, et al. Nodal, paranodal and juxtaparanodal axonal proteins during demyelination and remyelination in multiple sclerosis. Brain 2006;129:3186–95
16. Bedell MA, Jenkins NA, Copeland NG. Mouse models of human disease. Part I: Techniques and resources for genetic analysis in mice. Genes Dev 1997;11:1–10
17. Bedell MA, Largaespada DA, Jenkins NA, et al. Mouse models of human disease. Part II: Recent progress and future directions. Genes Dev 1997;11:11–43
18. Oliver PL, Davies KE. Analysis of human neurological disorders using mutagenesis in the mouse. Clin Sci (Lond) 2005;108:385–97
19. Einheber S, Zanazzi G, Ching W, et al. The axonal membrane protein Caspr, a homologue of neurexin IV, is a component of the septate-like paranodal junctions that assemble during myelination. J Cell Biol 1997; 139:1495–506
20. Menegoz M, Gaspar P, Le Bert M, et al. Paranodin, a glycoprotein of neuronal paranodal membranes. Neuron 1997;19:319–31
21. Bellen HJ, Lu Y, Beckstead R, et al. Neurexin IV, caspr and paranodin—novel members of the neurexin family: Encounters of axons and glia. Trends Neurosci 1998;21:444–49
22. Green EL. Linkage of Shambling with Rex in linkage group VII of the mouse. J Heredity 1968;59:59
23. Chomczynski P, Sacchi N. Single-step method of RNA isolation by acid guanidinium thiocyanate-phenol-chloroform extraction. Anal Biochem 1987;162:156–59
24. Murata Y, Seo H, Sekiguchi K, et al. Specific induction of fibronectin gene in rat liver by thyroid hormone. Mol Endocrinol 1990;4:693–99
25. Poliak S, Gollan L, Martinez R, et al. Caspr2, a new member of the neurexin superfamily, is localized at the juxtaparanodes of myelinated axons and associates with K+ channels. Neuron 1999;24: 1037–47
26. Peles E, Nativ M, Lustig M, et al. Identification of a novel contactin-associated transmembrane receptor with multiple domains implicated in protein-protein interactions. EMBO J 1997;16:978–88
27. Paintal A. Effects of temperature on conduction in single vagal and saphenous myelinated nerve fibres of the cat. J Physiol 1965;180:20–49
28. Gollan L, Sabanay H, Poliak S, et al. Retention of a cell adhesion complex at the paranodal junction requires the cytoplasmic region of Caspr. J Cell Biol 2002;157:1247–56
29. Faivre-Sarrailh C, Gauthier F, Denisenko-Nehrbass N, et al. The glycosylphosphatidyl inositol–anchored adhesion molecule F3/contactin is required for surface transport of paranodin/contactin-associated protein (caspr). J Cell Biol 2000;149:491–502
30. Bonnon C, Bel C, Goutebroze L, et al. PGY repeats and N-glycans govern the trafficking of paranodin and its selective association with contactin and neurofascin-155. Mol Biol Cell 2007;18:229–41
31. Falk J, Bonnon C, Girault JA, et al. F3/contactin, a neuronal cell adhesion molecule implicated in axogenesis and myelination. Biol Cell 2002;94:327–34
32. Rios JC, Melendez-Vasquez CV, Einheber S, et al. Contactin-associated protein (Caspr) and contactin form a complex that is targeted to the paranodal junctions during myelination. J Neurosci 2000;20:8354–64
33. Charles P, Tait S, Faivre-Sarrailh C, et al. Neurofascin is a glial receptor for the paranodin/Caspr-contactin axonal complex at the axoglial junction. Curr Biol 2002;12:217–20
34. Gollan L, Salomon D, Salzer JL, et al. Caspr regulates the processing of contactin and inhibits its binding to neurofascin. J Cell Biol 2003;163: 1213–18
35. Green EL. Shambling, a neurological mutant of the mouse. J Heredity 1967;58:65–68
36. Mendell JT, Dietz HC. When the message goes awry: Disease-producing mutations that influence mRNA content and performance. Cell 2001; 107:411–14
37. Maquat LE. Nonsense-mediated mRNA decay. Curr Biol 2002;12: R196–97
38. Poliak S, Gollan L, Salomon D, et al. Localization of Caspr2 in myelinated nerves depends on axon-glia interactions and the generation of barriers along the axon. J Neurosci 2001;21:7568–75
39. Chiappa KH, Yiannikas C. Voluntary alteration of evoked potentials? Ann Neurol 1982;12:496–97
40. Hume AL, Waxman SG. Evoked potentials in suspected multiple sclerosis: Diagnostic value and prediction of clinical course. J Neurol Sci 1988;83:191–210
41. Martin M, Hiltner TD, Wood JC, et al. Myelin deficiencies visualized in vivo: Visually evoked potentials and T2-weighted magnetic resonance images of shiverer mutant and wild-type mice. J Neurosci Res 2006;84: 1716–26
42. Venken K, Meuleman J, Irobi J, et al. *Caspr1/paranodin/neurexin IV* is most likely not a common disease-causing gene for inherited peripheral neuropathies. Neuroreport 2001;12:2609–14

